The Astrophysical Journal, 787:15 (13pp), 2014 May 20 doi:10.1088/0004-637X/787/1/15

HIGH-ENERGY GAMMA-RAY EMISSION FROM SOLAR FLARES: SUMMARY OF *FERMI* LARGE AREA TELESCOPE DETECTIONS AND ANALYSIS OF TWO M-CLASS FLARES

M. Ackermann[1], M. Ajello[2], A. Albert[3], A. Allafort[4], L. Baldini[5], G. Barbiellini[6,7], D. Bastieri[8,9], K. Bechtol[4], R. Bellazzini[10], E. Bissaldi[11], E. Bonamente[12,13], E. Bottacini[4], A. Bouvier[14], T. J. Brandt[15], J. Bregeon[10], M. Brigida[16,17], P. Bruel[18], R. Buehler[4], S. Buson[8,9], G. A. Caliandro[19], R. A. Cameron[4], P. A. Caraveo[20], C. Cecchi[12,13], E. Charles[4], A. Chekhtman[21,56], Q. Chen[4], J. Chiang[4], G. Chiaro[9], S. Ciprini[22,23], R. Claus[4], J. Cohen-Tanugi[24], J. Conrad[25,26,27,57], S. Cutini[22,23], F. D'Ammando[28], A. de Angelis[29], F. de Palma[16,17], C. D. Dermer[30], R. Desiante[6], S. W. Digel[4], L. Di Venere[4], E. do Couto e Silva[4], P. S. Drell[4], A. Drlica-Wagner[4], C. Favuzzi[16,17], S. J. Fegan[18], W. B. Focke[4], A. Franckowiak[4], Y. Fukazawa[31], S. Funk[4], P. Fusco[16,17], F. Gargano[17], D. Gasparrini[22,23], S. Germani[12,13], N. Giglietto[16,17], F. Giordano[16,17], M. Giroletti[28], T. Glanzman[4], G. Godfrey[4], I. A. Grenier[32], J. E. Grove[30], S. Guiriec[15], D. Hadasch[19], M. Hayashida[4,33], E. Hays[15], D. Horan[18], R. E. Hughes[3], Y. Inoue[4], M. S. Jackson[26,34], T. Jogler[4], G. Jóhannesson[35], W. N. Johnson[30], T. Kamae[4], T. Kawano[31], J. Knödlseder[36,37], M. Kuss[10], J. Lande[4], S. Larsson[25,26,38], L. Latronico[39], M. Lemoine-Goumard[40,58], F. Longo[6,7], F. Loparco[16,17], B. Lott[40], M. N. Lovellette[30], P. Lubrano[12,13], M. Mayer[1], M. N. Mazziotta[17], J. E. McEnery[15,41], P. F. Michelson[4], T. Mizuno[42], A. A. Moiseev[41,43], C. Monte[16,17], M. E. Monzani[4], E. Moretti[26,34], A. Morselli[44], I. V. Moskalenko[4], S. Murgia[4], R. Murphy[30], R. Nemmen[15], E. Nuss[24], M. Ohno[45], T. Ohsugi[42], A. Okumura[4,46], N. Omodei[4], M. Orienti[28], E. Orlando[4], J. F. Ormes[47], D. Paneque[4,48], J. H. Panetta[4], J. S. Perkins[15,43,49,50], M. Pesce-Rollins[10], V. Petrosian[4], F. Piron[24], G. Pivato[9], T. A. Porter[4], S. Rainò[16,17], R. Rando[8,9], M. Razzano[10,14], A. Reimer[4,11], O. Reimer[4,11], S. Ritz[14], A. Schulz[1], C. Sgrò[10], E. J. Siskind[51], G. Spandre[10], P. Spinelli[16,17], H. Takahashi[31], Y. Takeuchi[52], Y. Tanaka[45], J. G. Thayer[4], J. B. Thayer[4], D. J. Thompson[15], L. Tibaldo[4], M. Tinivella[10], G. Tosti[12,13], E. Troja[15,59], V. Tronconi[9], T. L. Usher[4], J. Vandenbroucke[4], V. Vasileiou[24], G. Vianello[4,53], V. Vitale[44,54], M. Werner[11], B. L. Winer[3], D. L. Wood[55,56], K. S. Wood[30], M. Wood[4], and Z. Yang[25,26]

[1] Deutsches Elektronen Synchrotron DESY, D-15738 Zeuthen, Germany
[2] Space Sciences Laboratory, 7 Gauss Way, University of California, Berkeley, CA 94720-7450, USA
[3] Department of Physics, Center for Cosmology and Astro-Particle Physics, The Ohio State University, Columbus, OH 43210, USA
[4] W. W. Hansen Experimental Physics Laboratory, Kavli Institute for Particle Astrophysics and Cosmology, Department of Physics and SLAC National Accelerator Laboratory, Stanford University, Stanford, CA 94305, USA; allafort@stanford.edu, nicola.omodei@stanford.edu, vahep@stanford.edu
[5] Università di Pisa and Istituto Nazionale di Fisica Nucleare, Sezione di Pisa, I-56127 Pisa, Italy
[6] Istituto Nazionale di Fisica Nucleare, Sezione di Trieste, I-34127 Trieste, Italy
[7] Dipartimento di Fisica, Università di Trieste, I-34127 Trieste, Italy
[8] Istituto Nazionale di Fisica Nucleare, Sezione di Padova, I-35131 Padova, Italy
[9] Dipartimento di Fisica e Astronomia "G. Galilei," Università di Padova, I-35131 Padova, Italy
[10] Istituto Nazionale di Fisica Nucleare, Sezione di Pisa, I-56127 Pisa, Italy
[11] Institut für Astro- und Teilchenphysik and Institut für Theoretische Physik, Leopold-Franzens-Universität Innsbruck, A-6020 Innsbruck, Austria
[12] Istituto Nazionale di Fisica Nucleare, Sezione di Perugia, I-06123 Perugia, Italy
[13] Dipartimento di Fisica, Università degli Studi di Perugia, I-06123 Perugia, Italy
[14] Santa Cruz Institute for Particle Physics, Department of Physics and Department of Astronomy and Astrophysics, University of California at Santa Cruz, Santa Cruz, CA 95064, USA
[15] NASA Goddard Space Flight Center, Greenbelt, MD 20771, USA
[16] Dipartimento di Fisica "M. Merlin" dell'Università e del Politecnico di Bari, I-70126 Bari, Italy
[17] Istituto Nazionale di Fisica Nucleare, Sezione di Bari, I-70126 Bari, Italy; nico.giglietto@ba.infn.it
[18] Laboratoire Leprince-Ringuet, École polytechnique, CNRS/IN2P3, F-91128 Palaiseau, France
[19] Institut de Ciències de l'Espai (IEEE-CSIC), Campus UAB, E-08193 Barcelona, Spain
[20] INAF-Istituto di Astrofisica Spaziale e Fisica Cosmica, I-20133 Milano, Italy
[21] Center for Earth Observing and Space Research, College of Science, George Mason University, Fairfax, VA 22030, USA
[22] Agenzia Spaziale Italiana (ASI) Science Data Center, I-00044 Frascati (Roma), Italy
[23] Istituto Nazionale di Astrofisica-Osservatorio Astronomico di Roma, I-00040 Monte Porzio Catone (Roma), Italy
[24] Laboratoire Univers et Particules de Montpellier, Université Montpellier 2, CNRS/IN2P3, F-34095 Montpellier, France
[25] Department of Physics, Stockholm University, AlbaNova, SE-106 91 Stockholm, Sweden
[26] The Oskar Klein Centre for Cosmoparticle Physics, AlbaNova, SE-106 91 Stockholm, Sweden
[27] The Royal Swedish Academy of Sciences, Box 50005, SE-104 05 Stockholm, Sweden
[28] INAF Istituto di Radioastronomia, I-40129 Bologna, Italy
[29] Dipartimento di Fisica, Università di Udine and Istituto Nazionale di Fisica Nucleare, Sezione di Trieste, Gruppo Collegato di Udine, I-33100 Udine, Italy
[30] Space Science Division, Naval Research Laboratory, Washington, DC 20375-5352, USA
[31] Department of Physical Sciences, Hiroshima University, Higashi-Hiroshima, Hiroshima 739-8526, Japan
[32] Laboratoire AIM, CEA-IRFU/CNRS/Université Paris Diderot, Service d'Astrophysique, CEA Saclay, F-91191 Gif sur Yvette, France
[33] Department of Astronomy, Graduate School of Science, Kyoto University, Sakyo-ku, Kyoto 606-8502, Japan
[34] Department of Physics, Royal Institute of Technology (KTH), AlbaNova, SE-106 91 Stockholm, Sweden
[35] Science Institute, University of Iceland, IS-107 Reykjavik, Iceland
[36] CNRS, IRAP, F-31028 Toulouse cedex 4, France
[37] GAHEC, Université de Toulouse, UPS-OMP, IRAP, F-31100 Toulouse, France
[38] Department of Astronomy, Stockholm University, SE-106 91 Stockholm, Sweden
[39] Istituto Nazionale di Fisica Nucleare, Sezione di Torino, I-10125 Torino, Italy
[40] Centre d'Études Nucléaires de Bordeaux Gradignan, Université Bordeaux 1, CNRS/IN2p3, F-33175 Gradignan, France
[41] Department of Physics and Department of Astronomy, University of Maryland, College Park, MD 20742, USA

[42] Hiroshima Astrophysical Science Center, Hiroshima University, Higashi-Hiroshima, Hiroshima 739-8526, Japan
[43] Center for Research and Exploration in Space Science and Technology (CRESST) and NASA Goddard Space Flight Center, Greenbelt, MD 20771, USA
[44] Istituto Nazionale di Fisica Nucleare, Sezione di Roma "Tor Vergata," I-00133 Roma, Italy
[45] Institute of Space and Astronautical Science, JAXA, 3-1-1 Yoshinodai, Chuo-ku, Sagamihara, Kanagawa 252-5210, Japan; tanaka@astro.isas.jaxa.jp
[46] Solar-Terrestrial Environment Laboratory, Nagoya University, Nagoya 464-8601, Japan
[47] Department of Physics and Astronomy, University of Denver, Denver, CO 80208, USA
[48] Max-Planck-Institut für Physik, D-80805 München, Germany
[49] Department of Physics and Center for Space Sciences and Technology, University of Maryland Baltimore County, Baltimore, MD 21250, USA
[50] Harvard-Smithsonian Center for Astrophysics, Cambridge, MA 02138, USA
[51] NYCB Real-Time Computing Inc., Lattingtown, NY 11560-1025, USA
[52] Research Institute for Science and Engineering, Waseda University, 3-4-1 Okubo, Shinjuku, Tokyo 169-8555, Japan
[53] Consorzio Interuniversitario per la Fisica Spaziale (CIFS), I-10133 Torino, Italy
[54] Dipartimento di Fisica, Università di Roma "Tor Vergata," I-00133 Roma, Italy
[55] Praxis Inc., Alexandria, VA 22303, USA
Received 2013 April 12; accepted 2014 March 24; published 2014 April 29

ABSTRACT

We present the detections of 18 solar flares detected in high-energy γ-rays (above 100 MeV) with the *Fermi* Large Area Telescope (LAT) during its first 4 yr of operation. This work suggests that particle acceleration up to very high energies in solar flares is more common than previously thought, occurring even in modest flares, and for longer durations. Interestingly, all these flares are associated with fairly fast coronal mass ejections (CMEs). We then describe the detailed temporal, spatial, and spectral characteristics of the first two long-lasting events: the 2011 March 7 flare, a moderate (M3.7) impulsive flare followed by slowly varying γ-ray emission over 13 hr, and the 2011 June 7 M2.5 flare, which was followed by γ-ray emission lasting for 2 hr. We compare the *Fermi* LAT data with X-ray and proton data measurements from *GOES* and *RHESSI*. We argue that the γ-rays are more likely produced through pion decay than electron bremsstrahlung, and we find that the energy spectrum of the proton distribution softens during the extended emission of the 2011 March 7 flare. This would disfavor a trapping scenario for particles accelerated during the impulsive phase of the flare and point to a continuous acceleration process at play for the duration of the flares. CME shocks are known for accelerating the solar energetic particles (SEPs) observed in situ on similar timescales, but it might be challenging to explain the production of γ-rays at the surface of the Sun while the CME is halfway to the Earth. A stochastic turbulence acceleration process occurring in the solar corona is another likely scenario. Detailed comparison of characteristics of SEPs and γ-ray-emitting particles for several flares will be helpful to distinguish between these two possibilities.

Key words: Sun: flares – Sun: X-rays, gamma rays

Online-only material: color figures

1. INTRODUCTION

Solar flares are explosive phenomena that emit electromagnetic radiation extending from radio to γ-rays. It is generally agreed that magnetic energy stored in the solar corona and released through reconnection is the source of plasma heating and acceleration of electrons and ions to relativistic energies. Measurements of hard X-rays (HXRs) up to ~300 keV indicate the presence of electrons with energies up to a few MeV producing bremsstrahlung in the high-density regions of the solar corona and chromosphere. Microwave observations indicate synchrotron emission by higher-energy, relativistic electrons in ~100 G magnetic fields. In some flares, often *GOES* (*Geostationary Operational Environmental Satellite*) X-class, electron bremsstrahlung emission is detected up to tens of MeV (e.g., Trottet et al. 1998). Nuclear γ-ray lines in the 1–10 MeV range and continuum radiation above 100 MeV produced by accelerated protons, α particles, and heavier ions have been detected with instruments on board the *Solar Maximum Mission* (*SMM*), the *Compton Gamma Ray Observatory* (*CGRO*), and *RHESSI* (Lin et al. 2002). The lines are due to de-excitation of ambient (or accelerated) ions excited by interactions with accelerated (or ambient) ions. The continuum radiation is produced by interactions of >300 MeV protons and >800 MeV α particles with ambient ions producing neutral and charged pions (Murphy et al. 1987). The neutral pions decay into a pair of 67.5 MeV γ-rays (in the rest frame of the pion), and the charged pions decay ultimately into energetic electrons, positrons, and neutrinos. The secondary electrons and positrons emit bremsstrahlung γ-rays in the tens of MeV energy range. These particles also produce inverse Compton X-rays by up-scattering solar optical photons and terahertz synchrotron radiation.

In general, the γ-ray emission light curve is similar to that of the HXRs (possibly with some delay), lasting for 10–100 s. This is referred to as the "impulsive" phase of the flare. However, the Energetic Gamma Ray Experiment Telescope (EGRET) on board *CGRO* (Kanbach et al. 1988; Esposito et al. 1999) detected γ-rays above 100 MeV for more than an hour after the impulsive phases of three flares (Ryan 2000). Among them, the 1991 June 11 flare is remarkable because the γ-ray emission (>50 MeV) lasted for 8 hr after the impulsive phase of the *GOES* X12.0 flare (Kanbach et al. 1993). The measured γ-ray spectrum appeared to be a composite of electron bremsstrahlung and pion-decay components (Kanbach et al. 1993; Rank et al. 2001; Ramaty & Mandzhavidze 1994). The γ-ray light curve showed a smooth exponential decay (Kanbach et al. 1993). Ryan (2000) suggested that the particles accelerated during the impulsive phase of the flare could remain trapped for the entire duration of the flare and precipitate gradually into the denser solar

[56] Resident at Naval Research Laboratory, Washington, DC 20375, USA.
[57] Royal Swedish Academy of Sciences Research Fellow, funded by a grant from the K. A. Wallenberg Foundation.
[58] Funded by contract ERC-StG-259391 from the European Community.
[59] NASA Postdoctoral Program Fellow, USA.

atmosphere to produce the γ-rays. Alternatively, continuous acceleration (Rank et al. 2001), either by a coronal mass ejection (CME) shock or by turbulence in a closed magnetic loop, is a possible origin.

As solar activity increases with the progress of the solar cycle, the Large Area Telescope (LAT; Atwood et al. 2009) and Gamma-ray Burst Monitor (GBM; Meegan et al. 2009) instruments on the *Fermi Gamma-Ray Space Telescope* are beginning to observe γ-rays and HXRs from solar flares. As we show below, in its first 4 yr of operation, the LAT has detected emission above 100 MeV in at least 18 flares. In this paper, we describe the continuous monitoring of the Sun that we perform with the LAT and outline broad conclusions that we derive from analysis of these flares. We then discuss in detail the first two long-duration flares: the *GOES* M-class flares SOL2011-03-07T20:12 and SOL2011-06-07T06:41. For both flares, the Sun was outside the field of view (FOV) of the LAT during the impulsive phase; nevertheless, a significant flux of γ-rays was detected when the Sun entered the LAT FOV at several intervals over the next ∼13 hr on March 7 and 8 and at one interval on June 7. Results of the temporal and spectral analyses and localization studies are described in Section 3, followed by a brief interpretation in Section 4.

2. DATA ANALYSIS

The *Fermi* LAT is a wide FOV, imaging telescope for high-energy γ-rays, designed to cover an energy range from 20 MeV up to more than 300 GeV (Atwood et al. 2009). The instrument consists of a precision tracker with silicon strip detectors above a cesium-iodide calorimeter. Both are enclosed in the plastic scintillators of the Anti-Coincidence Detector (ACD) that provides charged-particle tagging for background rejection. For bright solar flares an intense flux of X-rays during the impulsive phase of the flare can result in pulse pileup in the ACD scintillators within the integration time of the ACD readout. A coincident γ-ray entering the LAT within that integration time can be misidentified by the instrument's flight software or event-classification ground software as a charged particle and thereby mistakenly vetoed. During these periods, the nominal LAT instrument response functions do not apply, and the data cannot be analyzed by standard software. These issues were addressed in detail in Ackermann et al. (2012b) for the 2010 June 12 flare. The LAT instrument team closely monitors for this effect and tags such data as "bad" in the public data archive.[60] Data marked as "bad" have been included in the continuous monitoring of the Sun that we describe in Section 2.1. The goal of this monitoring is to detect any possible increase of the solar flux. (The effect of the ACD pileup is to decrease the effective collecting area; therefore, a significant excess will still correspond to an increase of the flux.) On the other hand, the instrument response functions (used for high-level analysis) do not account for this effect, and the value of the measured flux will not be correct during time intervals with high ACD pileup. We therefore remove such time intervals in the detailed analysis of standard LAT data (Section 2.2).

2.1. *LAT* `SunMonitor`

Fermi has spent more than 95% of its mission to date in survey mode, in which the spacecraft rocks to put the center of the LAT FOV 50° north and 50° south of the orbital equator on alternate orbits. In this way, the LAT monitors the entire sky every 2 orbits, or about every 3 hr, and observes the Sun for ∼20–40 contiguous minutes in that time (see Section 3.1). We have created an automated data analysis pipeline, the *Fermi*-LAT `SunMonitor`, to monitor the high-energy γ-ray flux from the Sun throughout the *Fermi* mission. The time intervals during which we run the analysis are the intervals in which the Sun is less than 60° off-axis for the LAT. In this way, each interval corresponds to the maximum time with continuous Sun exposure, and the durations of these intervals vary as the Sun advances along the ecliptic and as the orbit of *Fermi* precesses. We use γ-rays with energies between 100 MeV and 10 GeV from the `P7SOURCE_V6` event class (Ackermann et al. 2012a), which is commonly used for study of point sources in the LAT data and is well suited for point-source analysis.

Contamination from γ-rays produced by cosmic-ray interactions with the Earth's atmosphere is reduced by selecting events measured to be within 105° of the zenith. Each interval is analyzed using a region of interest (ROI) of 12° radius, centered on the position of the Sun at the central time of the interval. The maximum deviation of the true position of the Sun due to its apparent motion during these ∼30 minutes is less than 1′. This is smaller than the typical angular resolution of the instrument (the 68% containment angle of the reconstructed incoming γ-ray direction for normal incidence at 1 GeV is 0.°8 and at 100 MeV is 6°) and the localization precision for even bright solar flares. It is therefore not necessary to apply a correction to account for the motion of the Sun from the center of the ROI. However, for the analysis of long-duration flares, it becomes relevant (see Section 2.2).

In each time window, we perform a likelihood analysis that consists of maximizing the probability of obtaining the data given an input model. The ROI is modeled with a solar component and two templates for diffuse γ-ray background emission: a Galactic component produced by the interaction of cosmic rays with the gas and interstellar radiation fields of the Milky Way, and an isotropic component that includes both the contribution of the extragalactic diffuse emission and the residual cosmic rays that passed the γ-ray classification.[61] We fix the normalization of the Galactic component but leave the normalization of the isotropic background as a free parameter, to account for variable fluxes of residual cosmic rays.

Two additional backgrounds relevant for analyses of solar flares are the quiet-Sun emissions (Abdo et al. 2011) from cosmic-ray interactions with the Sun (disk) and with the solar radiation field. However, for the typical duration of the `SunMonitor` analysis (nominally less than an hour), these backgrounds are not significant. We verified that the background model describes the data well at times away from flares.

To test for transient solar emission, the Sun is assumed to be a point source with a γ-ray spectrum described by a power law with an exponential cutoff (see Section 3.3). The three spectral parameters are left free (in Section 3.3 we perform detailed spectral analyses using additional, physically motivated spectral forms).

All free parameters are fitted to maximize the likelihood, using the unbinned maximum likelihood algorithm `gtlike`.[62] We want to evaluate the significance of the potential flaring

[60] http://fermi.gsfc.nasa.gov/ssc/data/access/

[61] The models used for this analysis, `gal_2yearp7v6_v0.fits` and `iso_p7v6source.txt`, are available at http://fermi.gsfc.nasa.gov/ssc/data/access/lat/BackgroundModels.html.

[62] We used the `ScienceTools` version 09-28-00, available on the *Fermi* Science Support Center Web site http://fermi.gsfc.nasa.gov/ssc/. The `gtlike` documentation can be found here: http://fermi.gsfc.nasa.gov/ssc/data/analysis/scitools/help/gtlike.txt. The unbinned method is recommended for

signal and use the likelihood ratio test, or test statistic (TS) methods described in detail in Mattox et al. (1996). We compare $\mathcal{L}_0$, the likelihood of the null hypothesis (no "flare" present at the position of the Sun), and $\mathcal{L}$, the maximum likelihood when the source is added to the model and freely fitted, by computing $\mathrm{TS} = 2[\log \mathcal{L} - \log \mathcal{L}_0]$. To understand the statistical significance corresponding to a particular value of TS, we applied the `SunMonitor` analysis to a test location moving along the ecliptic plane 180° from the Sun for the full 4 yr data set (corresponding roughly to 10^4 realizations). Over such a long period, this fiducial location samples the same charged-particle and celestial backgrounds as the Sun but is free of any possible flare signal. The distribution of TS values determined for the test location was consistent with a chi-squared distribution with 2 degrees of freedom (or more precisely $1/2\ \chi^2_2$). From Wilks's theorem, we might naively expect, with the addition of three parameters (flux normalization, photon index, and cutoff energy), that TS would be distributed as χ^2_3. In our case, however, the factor of $1/2$ arises from the requirement that source flux not be negative, and the reduction in degrees of freedom from 3 to 2 results from correlation among model parameters.

Continuous monitoring of the Sun has led to the high-confidence detections of a number of flares with the LAT. In Table 1, we list detections for which the TS is greater than 30 (roughly corresponding to 5σ), along with estimates of their >100 MeV average flux during the indicated durations. We have grouped consecutive detections together into 15 distinct flaring episodes. To complement the results of the `SunMonitor`, we also analyzed the LAT Low Energy (LLE; Pelassa et al. 2010) data for every flare detected by *Fermi*-GBM, detecting three additional flares. These data have relaxed event selection compared to the data class used by the `SunMonitor` and are not compromised by pileup effects in the ACD during the impulsive phase of a flare. LLE analysis achieves larger effective area to transients in the 30 MeV to 1 GeV band than standard analysis. We have indicated the LLE detections during the impulsive phase using the label "LLE" in the TS column. Although it is possible to measure fluxes using LLE data (see, e.g., Ackermann et al. 2012b), a dedicated spectral analysis of each flare would be necessary. This is beyond the scope of this paper, and we defer to further publications for evaluation of the fluxes of LLE flares. CME shock speeds measured by Large Angle and Spectrometric Coronagraph Experiment (LASCO) on the *Solar and Heliospheric Observatory* (*SOHO*; Brueckner et al. 1995) are obtained from the *SOHO*/LASCO CME online catalog[63] and are reported in the fifth column of the table.

Several features are immediately apparent from the table. Although the `SunMonitor` has analyzed data since the start of the mission, the detection of solar flares starts only in mid-2010, with the rise of solar activity in the current cycle. In five cases, labeled as type "I" for "Impulsive" in the table, we detected the impulsive phase above 30 MeV using LLE data, and in two of them the flare was also detected above 100 MeV in standard likelihood analysis by the LAT `SunMonitor`. In some cases, due to the partial overlap between the duration of the *GOES* X-ray pulse and the time interval in which we detect the solar flare at high energy, we cannot disentangle the impulsive phase from the long-duration (or "Sustained") emission, and we have labeled these cases as type "I/S." When high-energy emission (>100 MeV) is detected in time intervals subsequent to the impulsive HXR emission, we have labeled the detections as type "S" for long-duration, "Sustained" emission. In three cases (2012 January 27, 2012 March 09, and 2012 March 10) the Sun was in the LAT FOV at the time of the HXR impulsive flare, but the LAT did not detect it, suggesting that high-energy emission can also arise at later times. We have labeled these type "D" for "Delayed." Although these cases are rare, they are particularly interesting and will be the subject of further analysis in a subsequent paper.

In almost all the cases, the flares are associated with moderately bright X-ray flares, although unlike the EGRET-detected flares, not all are X-class. Instead, they are predominantly M-class, and in one case (2011 June 2), high-energy emission occurred coincidentally with a series of C-class flares. All the flares are solar eruptive events (SEEs), i.e., they are associated with CMEs and solar energetic particles (SEPs). Most have fast ($\gtrsim$500 km s^{-1}) CMEs, and six have CME velocities $\sim$2000 km s^{-1}. The total energy radiated in >100 MeV γ-rays varies from $<10^{22}$ to 10^{25} erg and thus spans a broader dynamic range than other characteristics (e.g., *GOES* flux spans two decades, CME speed a factor of four, etc.). It is nonetheless small compared to the typical total energy of a flare, which can be $\gtrsim 10^{32}$ erg for the largest flares, attesting to the high sensitivity of the *Fermi* LAT. We caution that flares whose only high-energy emission is during the impulsive phase can be missed because of the modest in-aperture viewing fraction afforded by the sky survey observing strategy. Averaged over a year, the Sun is within the LAT FOV $\sim$20% of the time, and only a small number of flares are viewed during their impulsive phase. An example of this is the X5.4 flare on 2012 March 7, whose main impulsive burst was missed by *Fermi*.

2.2. Detailed Analysis of Two Flares

A detailed and complete analysis of all the flares in Table 1 is beyond the scope of this paper. Ackermann et al. (2012b) discuss a flare that exhibited only impulsive emission (<1 minute in duration) at high energies, the M2.0 flare of 2010 June 12, which showed γ-ray lines below 10 MeV and continuum up to 300 MeV in the LAT. Here we focus on the first two long-duration flares: the M3.7 solar flare of 2011 March 7, which was detected with LAT over an interval of almost 14 hr (Allafort et al. 2011), and the M2.5 flare of 2011 June 7 (Tanaka et al. 2011), detected for less than an hour. For these two flares, we used the same event class data as for the `SunMonitor` analysis and the corresponding instrument response functions (`P7SOURCE_V6`) in the 60 MeV to 6 GeV energy range for spectral analysis and the 100 MeV to 6 GeV range for localization. We restricted the data set to γ-rays arriving with zenith angles less than 100° to minimize contamination from atmospheric γ-rays, and we analyzed γ-rays within a 12° ROI around the Sun. We included the azimuthal (ϕ) dependence of the effective area of the LAT when calculating the exposure for the likelihood analysis. While the ϕ dependence averages out for observing timescales of days and longer, on scales of minutes and hours—relevant to solar flare analysis—the range of ϕ angle for an individual source is not well represented by the azimuthal average: e.g., the effective area can differ from the azimuthal averaged by 5% typically

time series analysis of the *Fermi* LAT data, where the number of events in each time bin is expected to be small.

[63] The CME catalog is generated and maintained at the CDAW Data Center by NASA and the Catholic University of America in cooperation with the Naval Research Laboratory. *SOHO* is a project of international cooperation between ESA and NASA.

Table 1
Solar Flares Detected by the *Fermi* LAT from 2008 August to 2012 August

Date	*GOES* X-Ray Class, Start–End[d]	Type	Duration (hr)	CME Speed[a] (km s^{-1})	*Fermi* Time Window Start[d], Duration (minutes)	TS[b]	Flux[c]	Energy Flux[c]
2010 Jun 12	M2.0, 00:30-01:02	I	···	486	00:55, 0.8	LLE[e]	···	···
2011 Mar 7	M3.7, 19:43-20:58	I/S	10.7	2125	20:15, 25	230	1.9 ± 0.3	6.7 ± 1.0
		S			23:26, 36	520	3.5 ± 0.3	11.9 ± 1.1
2011 Mar 8		S			02:38, 35	450	3.5 ± 0.3	11.6 ± 1.1
					05:49, 35	200	1.9 ± 0.3	5.4 ± 0.7
2011 Jun 2	C2.7,9:42-9:50	I/S	0.8	976	09:43, 45	35	0.4 ± 0.2	1.4 ± 0.5
2011 Jun 7	M2.5, 06:16-06:59	S	2.2	1255	07:34, 53	570	3.6 ± 0.3	11 ± 0.9
2011 Aug 4	M9.3, 03:41-04:04	S	1.9	1315	04:59, 34	390	2.5 ± 0.3	7.9 ± 0.8
2011 Aug 9	X6.9, 07:48-08:08	I	···	1610	08:01, 3.3	LLE[e]	···	···
2011 Sep 6	X2.1, 22:12-22:24	I	0.6	575	22:17, 0.2	LLE[e]	···	···
		I/S			22:13, 35	[f]	[f]	
2011 Sep 7	X1.8, 22:32-22:44	S	2.1	792	23:36, 63	350	1.0 ± 0.1	3.5 ± 0.4
2011 Sep 24	X1.9, 09:21-09:48	I	···	1936	09:34, 0.8	LLE[e]	···	···
2012 Jan 23	M8.7, 03:38-04:34	I/S	5.7	1953	04:07, 51	180	0.8 ± 0.1	2.7 ± 0.4
		S			05:25, 69	650	2.1 ± 0.2	6.6 ± 0.5
		S			07:26, 16	69	3.7 ± 0.9	9.6 ± 2.2
		S			08:47, 35	97	2.6 ± 0.5	7.0 ± 1.3
2012 Jan 27	X1.7, 17:37-18:56	D	4.0	1930	19:45, 11	78	3.2 ± 0.8	9.6 ± 2.2
		S			21:13, 24	47	1.0 ± 0.3	2.8 ± 0.8
2012 Mar 5	X1.1, 02:30-04:43	I/S	5.3	1602	04:12, 49	69	0.5 ± 0.1	1.5 ± 0.3
		S			05:26, 71	250	0.9 ± 0.1	2.5 ± 0.3
		S			07:23, 28	39	0.8 ± 0.2	2.4 ± 0.7
2012 Mar 7	X5.4, 00:02-00:40	S	20.2	2684	00:46, 31	22000	[f]	[f]
	X1.3, 01:05–01:23	I/S		1785	00:46, 60	LLE[g]	···	···
					03:56, 32	16000	113.1 ± 2.0	400.5 ± 6.6
					07:07, 32	8900	71.9 ± 1.6	232.6 ± 4.9
					10:18, 32	1900	30.1 ± 1.5	91.9 ± 4.3
					13:29, 32	120	8.9 ± 1.9	29.9 ± 5.9
					19:51, 25	50	0.4 ± 0.1	1.7 ± 0.5
2012 Mar 9	M6.3, 03:22-04:18	D	5.7	844	05:17, 34	51	0.6 ± 0.2	2.0 ± 0.5
		S			06:52, 35	100	0.9 ± 0.2	2.8 ± 0.6
		S			08:28, 34	159	1.4 ± 0.2	4.3 ± 0.7
2012 Mar 10	M8.4, 17:15-18:30	D	4.3	1379	21:05, 30	43	0.4 ± 0.1	1.0 ± 0.3
2012 May 17	M5.1, 01:25-02:14	I/S	1.2	1582	02:18, 22	45	1.0 ± 0.3	3.4 ± 0.9
2012 Jun 3	M3.3, 17:48-17:57	I	0.2	605	17:52, 0.6	LLE[e]	···	···
		I/S			17:40, 23	300	3.2 ± 0.4	10.6 ± 1.2
2012 Jul 6	X1.1,23:15-23:49	I/S	0.9	892	23:19, 52	930	3.5 ± 0.2	10.4 ± 0.7

Notes.
[a] CME data are available at the following url: http://cdaw.gsfc.nasa.gov/CME_list/.
[b] The significance of the detection in terms of σ is roughly $\sqrt{\mathrm{TS}}$.
[c] Flux and energy flux are calculated between 100 MeV and 10 GeV and have units of $\times 10^{-5}$ photons cm^{-2} s^{-1} and $\times 10^{-9}$ erg cm^{-2} s^{-1}, respectively.
[d] In UT, hour:minute format.
[e] LLE detections are for $E > 30$ MeV. Durations are evaluated from the LLE light curve above 30 MeV.
[f] The flux estimate is unreliable because of X-ray pileup in the ACD.
[g] Signal in LLE data is detected during the entire orbit; therefore, the reported duration is only a lower limit. See *Fermi*-LAT Collaboration (2013) for more details about this flare.

and more than 10% below 100 MeV or far off-axis (incidence angle $>60^{\circ}$).[64]

It is important to account for the apparent motion of the Sun in the analyses of particularly long flares, i.e., when this motion is a non-negligible fraction of the localization accuracy that is a tighter constraint than the size of the LAT point-spread function. Such is the case in analyzing the ∼14 hr of γ-ray emission from the March 7 event as a whole. (It is not necessary for the June 7 event since the high-energy emission was visible by LAT for only 36 minutes.) We have developed a dedicated "Sun-centering" analysis tool for moving sources. We transform the directions of all the γ-rays into ecliptic coordinates and

[64] http://fermi.gsfc.nasa.gov/ssc/data/analysis/documentation/Cicerone/Cicerone_LAT_IRFs for more details.

then translate them into ecliptic longitude to keep the Sun at position (0,0) as time passes. We apply the same operation to the pointing history of the LAT to keep an accurate account of the exposure. In Sun-centered coordinates the diffuse backgrounds are well approximated by an isotropic intensity. We verified that fitting the standard isotropic template to the data with a free normalization coefficient provides a good representation of the backgrounds. For long-duration flares (such as the March 7), or for detailed localization analysis, it is important to account for the steady solar disk component as a background source, which we had neglected in the `SunMonitor` analysis. We model the disk component of the quiet-Sun emission as a point source at the position of the center of the disk with the parameters fixed to their measured values (Abdo et al. 2011).

Uncertainties in the calibration of the LAT introduce systematic errors on the measurements. Effective area uncertainty is dominant, and for the `P7SOURCE_V6` event class it is estimated to be ∼10% at 100 MeV, decreasing to ∼5% at 560 MeV, and increasing to ∼10% at 10 GeV and above. In order to estimate the systematic uncertainties in the model parameters, we repeat the analysis using a set of custom modified instrument response functions. This technique, called "bracketing," is described in detail in Ackermann et al. (2012a).

3. RESULTS

On 2011 March 7, the solar activity increased dramatically, with a dozen M-class solar flares detected during the subsequent two days with the *GOES* soft X-ray monitor. Intense HXR emission (up to 300 keV) observed by *RHESSI* accompanied an M3.7 solar flare that erupted from the NOAA active region (AR) 11164 in the northwest quadrant. The impulsive phase started at about 19:43 UT and ended at 20:10 UT.[65] Around 6:16 UT on 2011 June 7, an M2.5 flare erupted from AR 11226 in the southwest quadrant, with prominent soft X-ray and HXR emission, ending at 06:59 UT.[66] The heliographic longitude of the flare site was similar to that of the March 7 flare. For both flares, the impulsive phase seen in HXRs by *RHESSI* occurred entirely while the Sun was outside the *Fermi* LAT FOV. Without any interference from the impulsive X-rays in the ACD, the *Fermi* LAT was able to start observing the Sun 33 and 92 minutes after the start of the March 7 and June 7 events, respectively.

3.1. Gamma-ray Light Curve

We used the output of the `SunMonitor` to identify the intervals during which significant emission was detected for the two flares. We then performed a more detailed spectral analysis for these intervals and the preceding and following six hour intervals. The upper panels of Figures 1 and 2 show the flux measurements or upper limits in each observing window, where each window is defined to be when the 12° radius analysis ROI (see Section 2) around the Sun is entirely within the 70° FOV. Table 2 gives the precise time and duration of each window in which we found a positive detection of emission at energies greater than 100 MeV. (Since the 2011 March 7 flare is detected with high significance in four consecutive time windows, we include also the last point with TS = 20.) The most striking feature of the March 7 flare is the slow increase of the flux, which reaches its peak, $F(>100\,\mathrm{MeV}) = (3.8 \pm 0.3) \times 10^{-5}$ photons s^{-1} cm^{-2}, more than 7 hr after the onset of the M3.7 flare itself. The flux then decreased gradually until the last significant detection, almost 14 hr after the impulsive phase. The June 7 flare was detected significantly only in the first observing window after the flare onset, with only upper limits obtained for the following windows. The flux measured in this first window, less than 2 hr after the impulsive phase, is of the same magnitude as the peak flux for the March 7 flare, with $F(>100\,\mathrm{MeV}) = (3.4 \pm 0.2) \times 10^{-5}$ photons cm^{-2} s^{-1}. The upper limits shown before and after the detections are consistent with the quiet-Sun flux of $(4.6 \pm 0.2) \times 10^{-7}$ photons cm^{-2} s^{-1} reported in Abdo et al. (2011).

We also searched for spectral evolution from one observing window to the next for the March 7 flare, as described in Section 3.3.

3.2. Localization

Localization of the high-energy γ-ray emission relative to the X-ray flaring site can provide valuable information about the source of the accelerated particles producing the high-energy emission. The key questions are whether that emission is tightly constrained to the flaring site, or displaced, or spatially extended. This is complicated by the fact that on March 7 and 8, within the 10 hr following the M3.7 flare from AR 11164, other regions of the Sun were active (AR 11165 and 11171), producing a total of three M-class flares (Figure 1, third panel). It is necessary to know the location of the source or sources of the γ-rays to interpret the light curve properly.

We used the maximum likelihood fitting package, `pointlike`, which was used in the localizations for the sources in the LAT 2 yr catalog (2FGL; Nolan et al. 2012). This tool maximizes the Poisson likelihood to reproduce the observed photon counts, in spatial and spectral bins, given a specific model for the source and backgrounds. `pointlike` is particularly suited for simultaneously fitting the position, spectrum, and possible spatial extension of a source (Kerr 2011; Lande et al. 2012). We limited this analysis to energies greater than 100 MeV to exclude γ-rays with the most uncertain directions. For both flares we investigated the possibility that the γ-ray emission is spatially extended, using a disk model and allowing the radius to be a free parameter in the global fit. We found no significant TS increase for an extended source relative to a point source, for either the total time of detection or individual intervals. Having no reason to pick a certain spatially extended template, we modeled the long-duration emission with a point source and found the best-fit source location for the full duration of the high-energy detection. Figure 3 shows the best locations, and corresponding circular 68% and 95% confidence statistical uncertainty regions are plotted for both flares on images of the Sun from the Atmospheric Imaging Assembly (AIA) on board the *Solar Dynamic Observatory* (*SDO*). Positions are expressed in Cartesian-projected heliographic coordinates. For the March 7 event, the best position is (750″, 690″) offset from the center of the solar disk with 68% and 95% confidence error radii of 290″ and 500″, respectively. This position in the northwest quadrant is consistent with that of AR 11164 as imaged by *RHESSI* and *SDO*. For June 7, the best location is (870″, −350″) with a 68% confidence radius of 500″, in the southwest quadrant of the solar disk and consistent with the position of AR 11226. The uncertainty is large because the source fluence is modest.

A possible bias in the determination of the position of an off-axis γ-ray source, particularly at low energy, is the so-called fisheye effect, a known systematic shift in the reconstruction

[65] http://www.swpc.noaa.gov/weekly/2011_WeeklyPDF/prf1854.pdf
[66] http://www.swpc.noaa.gov/weekly/2011_WeeklyPDF/prf1867.pdf

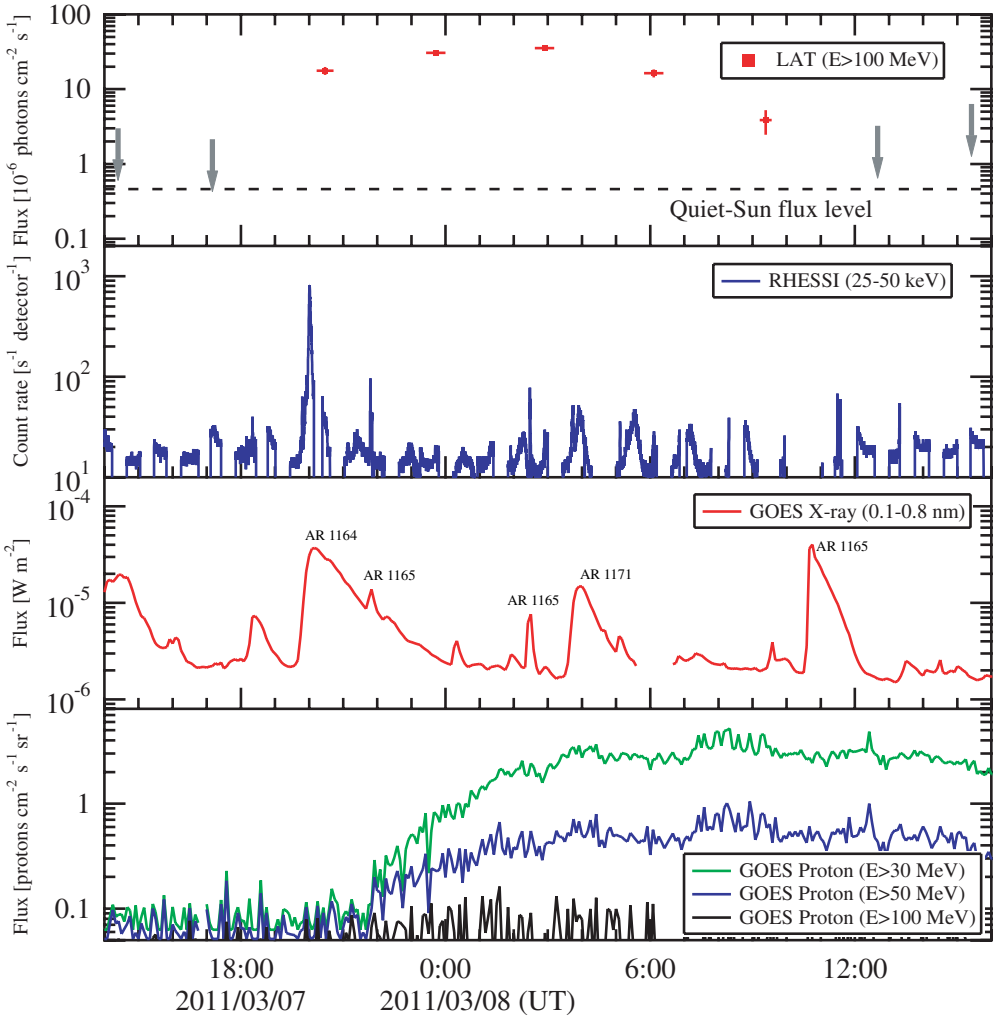

Figure 1. Multi-wavelength and proton light curves of *GOES* M3.7 SOL2011-03-07T20:12. γ-ray data are from the *Fermi* LAT, HXRs from *RHESSI*, and soft X-rays and protons from *GOES*. Vertical error bars of LAT data indicate 1σ statistical uncertainties, and gray arrows are 95% upper limits. The horizontal bar for each flux point represents the true duration over which the flux was computed (see Table 2), the Sun being out of the FOV at other times.

(A color version of this figure is available in the online journal.)

Table 2
Fermi LAT Observing Windows, Duration, γ-Ray Flux, and Best-fit Proton Spectral Index

Date (UT)	Duration (minutes)	Flux (>100 MeV) ($\times 10^{-5}$ photons cm^{-2} s^{-1})	Proton Index
GOES M3.7 flare, SOL2011-03-07T20:12			
2011 Mar 7 20:15:42.6	24	$1.7 \pm 0.2^{+0.2}_{-0.1}$	$4.0 \pm 0.5^{+0.2}_{-0.3}$
2011 Mar 7 23:26:51.6	33.5	$3.3 \pm 0.3^{+0.3}_{-0.2}$	$4.6 \pm 0.3^{+0.2}_{-0.2}$
2011 Mar 8 02:37:37.6	34	$3.5 \pm 0.3^{+0.3}_{-0.3}$	$4.9 \pm 0.3^{+0.2}_{-0.2}$
2011 Mar 8 05:49:03.6	34	$1.8 \pm 0.2^{+0.2}_{-0.1}$	>5.6
2011 Mar 8 09:13:06.7	21	$0.4 \pm 0.1^{+0.04}_{-0.03}$	[a]
GOES M2.5 flare, SOL2011-06-07T06:41			
2011 Jun 7 07:47:40	36	$3.1 \pm 0.2^{+0.3}_{-0.2}$	$4.3 \pm 0.3^{+0.2}_{-0.2}$

Notes. [a] In this time interval, the number of γ-rays is small and the pion-decay template spectrum does not produce a statistically satisfactory fit. The best-fit model to the γ-ray data is described by a power law with spectral index $\Gamma = 2.7 \pm 0.4$ with the reported flux.

of each event toward the center of the LAT FOV (Ackermann et al. 2012a). This bias does not affect long observations of steady sources with the LAT, but for short observations at high incidence angle, as is the case for most solar flares, this effect can be important, e.g., as we reported for the 2010 June 12 solar flare (Ackermann et al. 2012b). From Monte Carlo simulations we evaluated the energy-dependent correction to be applied to the incidence angle of each γ-ray, and for the March 7 flare the average shift of the reconstructed direction with respect to the Monte Carlo position is $\sim 100''$. This bias is negligible

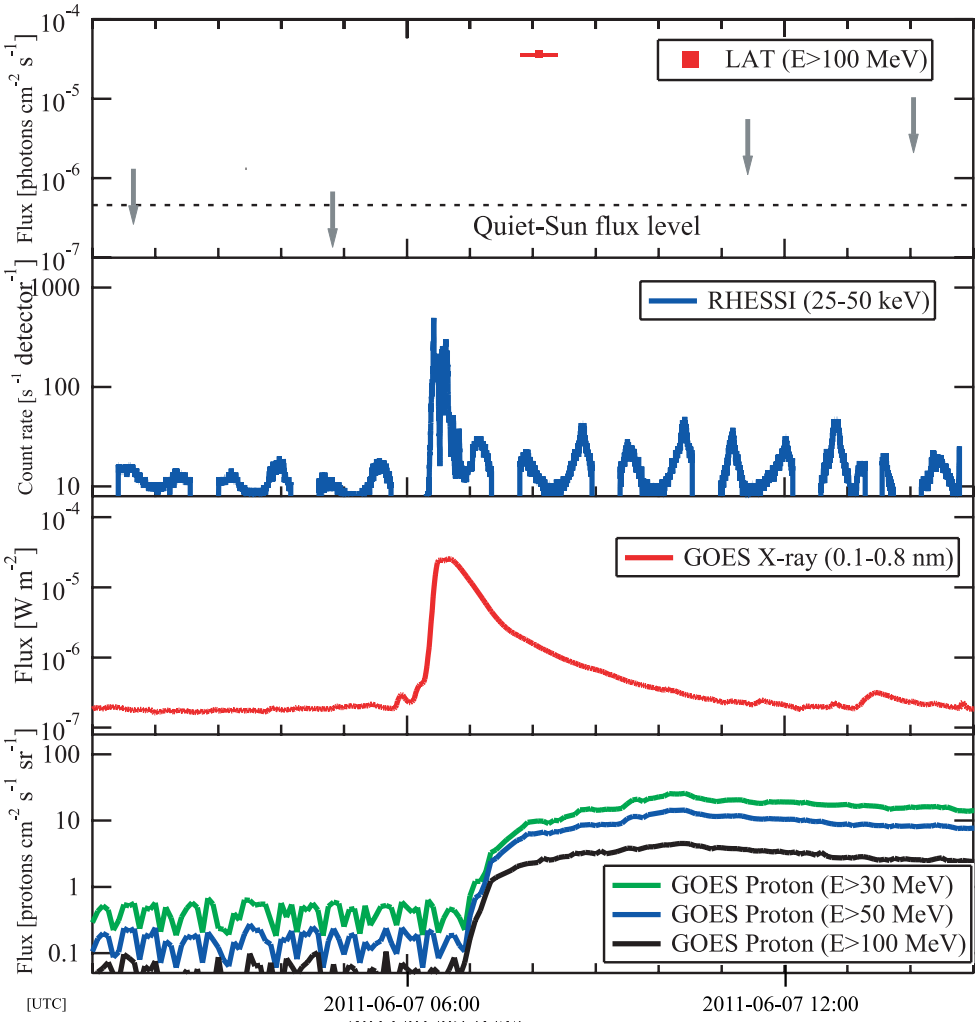

Figure 2. Multi-wavelength and proton light curves of *GOES* M2.5 SOL2011-06-07T06:41. γ-ray data are from the *Fermi* LAT, HXRs from *RHESSI*, and soft X-rays and protons from *GOES*. Vertical error bars of LAT data indicate 1σ statistical uncertainties, and gray arrows are 95% upper limits. The horizontal bar for each flux point represents the true duration over which the flux was computed (see Table 2), the Sun being out of the FOV at other times.

(A color version of this figure is available in the online journal.)

compared to statistical uncertainties, so we have not included it in the best-fit positions we reported above.

For the March 7 flare, we repeated the localization analysis for each observing window with a positive detection, but the low counting statistics produced large uncertainties that are not constraining and much larger than the solar disk. We were therefore unable to evaluate whether the high-energy emission site moved during the event.

3.3. Spectrum

We can evaluate the contributions from two distinct emission mechanisms, bremsstrahlung from accelerated electrons and decay of pions from interactions of accelerated hadrons, regardless of how the charged particles are accelerated, by comparing the >100 MeV data to model predictions. We used a simple power law $dN/d\epsilon = N_0\epsilon^{-\Gamma}$, where Γ is the photon index and ϵ the energy of the γ-rays, to describe bremsstrahlung from a power-law non-thermal electron distribution. To test whether the electron distribution breaks or cuts off at high energies, which would be reflected as a break or cutoff in the γ-ray distribution at lower energies, we also considered a power law with an exponential cutoff (ExpCutoff):

$$dN(\epsilon)/d\epsilon = N_0\epsilon^{-\Gamma}\exp(-\epsilon/\epsilon_{\rm co}). \quad (1)$$

Although the two models are identical only for $\epsilon_{\rm co} \rightarrow \infty$ and the likelihood-ratio test cannot be rigorously applied, we report in Table 3 the increment in TS obtained by including the exponential cutoff in the model. We also report the best-fit values of the parameters of the two models for both flares.

The power law with an exponential cutoff is a better representation of the γ-ray spectrum as the increment in TS value is greater than 25 in both cases. This simple analytic function is very similar to the γ-ray spectrum resulting from the decay of pions. For the pion-decay model, we used calculated γ-ray spectra resulting from interactions of protons and alpha particles having an isotropic momentum distribution and a power-law kinetic energy spectrum with index s [$dN_p(E)/dE \propto E^{-s}$] as described in Murphy et al. (1987). We obtained a series of tabulated photon spectra by varying the index s of the protons. We compared the associated pion-decay photon spectra with the data by performing an unbinned likelihood spectral analysis and computing the value of the logarithm of the likelihood

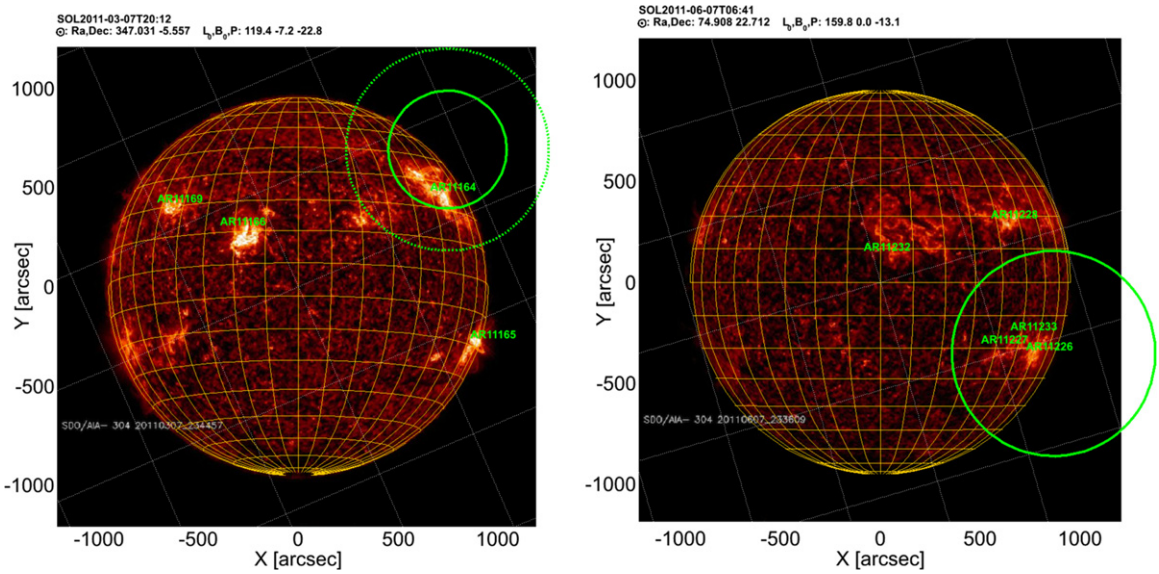

Figure 3. *Fermi* LAT localization of the high-energy emission (100 MeV–10 GeV) for the 2011 March 7 (left) and June 7 (right) flares. In each image, the Sun is displayed in heliographic coordinates, where the projection of the rotational axis of the Sun is along the *y*-axis, the *z*-axis is the line of sight (from the Sun to the observer), and the *x*-axis is the remaining orthogonal basis vector. The grid of constant heliographic latitude and longitude is yellow, and lines of constant R.A. and decl. (J2000) are white. The backgrounds are *SDO*/AIA images at 304 Å of the chromosphere and transition region around the Sun at the given epoch. The labels indicate the NOAA numbers of the active regions. The LAT localizations of the flares are shown by the green circles, solid and dashed lines at the 68% and 95% error radii, respectively.

(A color version of this figure is available in the online journal.)

Table 3
Best-fit Parameters with Statistical and Systematic Errors for the Time-integrated Spectra

Model		SOL2011-03-07T20:12	SOL2011-06-07T06:41
Power law	Flux[a]	$1.88 \pm 0.05 \pm 0.2$	$2.6 \pm 0.2 \pm 0.2$
	Γ	$2.56 \pm 0.06 \pm 0.08$	$2.45 \pm 0.09 \pm 0.08$
ExpCutoff	Flux[a]	$2.1 \pm 0.1 \pm 0.2$	$3.0 \pm 0.2^{+0.3}_{-0.2}$
	Γ	$1.5 \pm 0.3^{+0.05}_{-0.25}$	$1.1 \pm 0.4^{+0.1}_{-0.01}$
	ϵ_{co} (MeV)	$130 \pm 20^{+100}_{-1}$	$210 \pm 40^{+0.4}_{-50}$
	ΔTS[b]	96	44
Pion decay	Flux[a]	$2.1 \pm 0.1 \pm 0.2$	$3.1 \pm 0.2^{+0.3}_{-0.2}$
	Proton index	$4.5 \pm 0.2 \pm 0.2$	$4.3 \pm 0.3^{+0.2}_{-0.2}$

Notes.
[a] The integral flux between 100 MeV and 10 GeV is in units of 10^{-5} photons cm^{-2} s^{-1}.
[b] The TS increment for the exponential cutoff model is relative to the power-law model.

[log $\mathcal{L}$] with the normalization of the photon spectral template as a free parameter. To estimate the maximum likelihood proton index and its statistical uncertainty, we fit the values of $-\log \mathcal{L}$ calculated for the tabulated model spectra near their minima with a parabolic function of proton index s. The minimum gives the most likely index $s = s_0$ for the pion-decay model. We calculate the statistical uncertainty on the proton index using $\Delta\mathrm{TS} = 2[\log \mathcal{L}_s - \log \mathcal{L}_0] = 1$, which corresponds, by Wilks's theorem, to the 68% confidence level (CL) for a χ^2 distribution with 1 degree of freedom. In the last row of Table 3, we report the best-fit values of the proton spectral indices and their estimated uncertainties for both flares. Systematic errors are estimated using the bracketing method described in Ackermann et al. (2012a).

Figure 4 compares the observed and predicted number of γ-ray counts for different models for the March 7 and June 7 solar flares, while Figure 5 shows the reconstructed spectral energy distribution for the two flares. Numerical values of the flux with statistical errors are reported in Table 4. To obtain the 10 model-independent photon spectral data points, we fit the background through the entire energy range (60 MeV–6 GeV) and then, within each energy bin, determined the source flux using the *Fermi* Science Tool `gtlike` assuming a power-law photon

Table 4
Spectral Energy Distributions for the March 7 and June 7 Solar Flares

Energy Bin (MeV)	Flux ($\times 10^{-9}$ erg cm^{-2} s^{-1})	
	2011 March 7	2011 June 7
60–95	2.7 ± 0.4	2.5 ± 0.8
95–150	3.8 ± 0.4	5.3 ± 0.9
150–239	4.5 ± 0.4	7.7 ± 1.0
239–378	4.2 ± 0.4	4.6 ± 0.8
378–600	1.7 ± 0.3	3.7 ± 0.9
600–950	0.6 ± 0.2	<2.1
952–1508	<0.5	<1.3
1509–2391	<0.7	<1.9
2391–3789	<0.6	<4.1
3780–6000	<0.9	<4.0

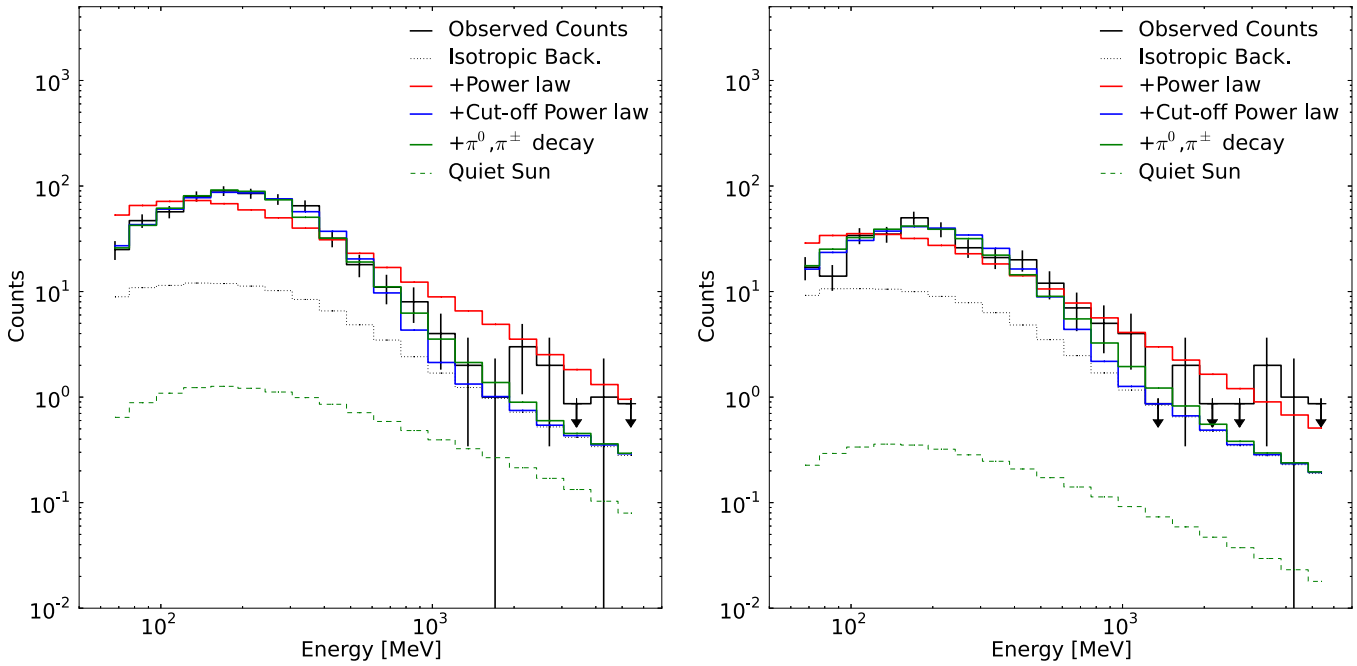

Figure 4. Comparison between observed γ-ray counts and predicted γ-ray counts for different models for the March 7 (left) and June 7 (right) solar flares. The black solid line is the histogram of the observed counts. Vertical bars are plotted using the Gehrels (1986) formula to show the expected uncertainty associated with each bin. Red, blue, and green solid lines are the expected numbers of counts for different models (background+power law, background+power law with exponential cutoff, and background+pion-decay, respectively) after likelihood maximization. The contribution of the quiet Sun is shown as a green dashed line (Abdo et al. 2011).

(A color version of this figure is available in the online journal.)

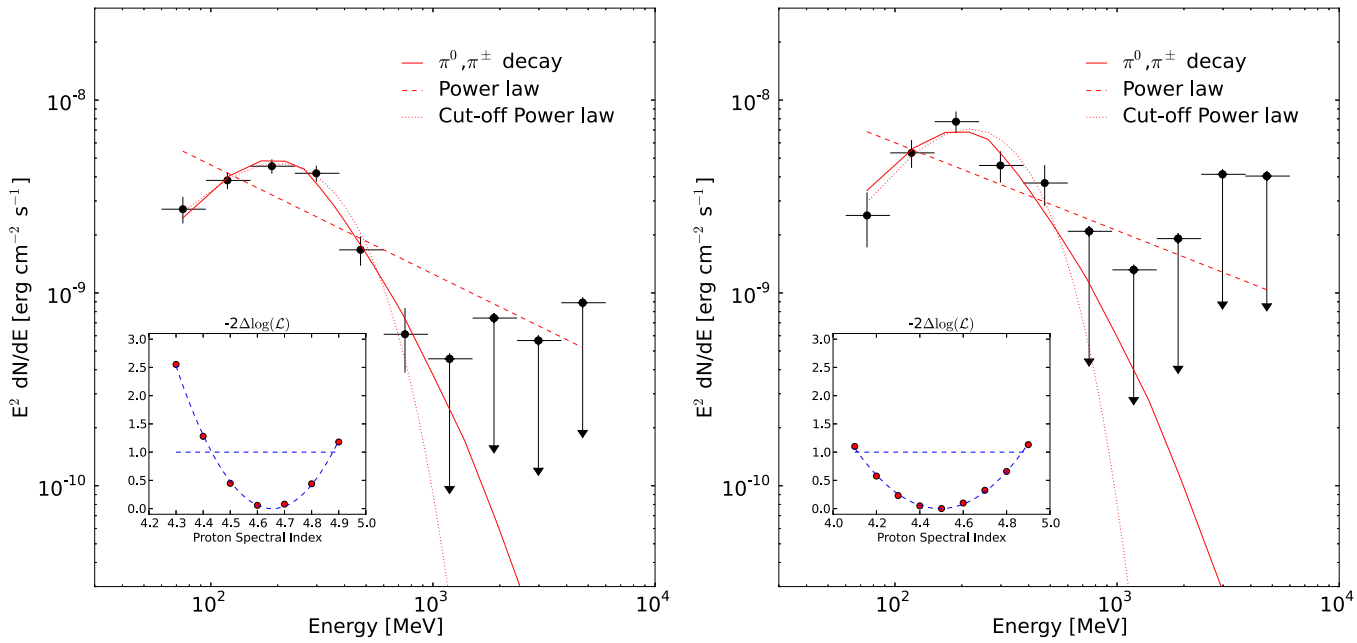

Figure 5. Reconstructed *Fermi* LAT spectral energy distributions of the March 7 (left) and June 7 (right) solar flares. The red solid, dotted, and dashed lines represent the pion-decay, exponential cutoff, and power-law models, respectively. Vertical bars indicate 1σ statistical uncertainties. Upper limits are computed at the 95% CL. The insets show the profile of the statistic $\Delta\mathrm{TS} = -2\Delta\log\mathcal{L}$ as a function of the proton spectral index used to calculate the pion-decay spectrum. The horizontal dashed lines at 1 indicate the value used to compute the uncertainty on the proton index corresponding to the 68% CL for a χ^2 distribution with 1 degree of freedom. Parameter values for the models obtained by maximizing the likelihood and used to evaluate the spectral fits shown above are in Table 3; flux measurements with statistical errors are reported in Table 4.

(A color version of this figure is available in the online journal.)

spectrum having fixed index of 2 and background parameters fixed at those obtained from the fit to the entire energy range. We note that the likelihood spectral fitting does not account for the finite energy resolution of the LAT ($\Delta E_{\mathrm{rms}} \approx 15\%$ at 100 MeV; Ackermann et al. 2012a; Atwood et al. 2009). The uncertainties on the energy measurement are smaller than the width of the spectral feature (curvature) we measure and therefore do not significantly affect our results.

Figure 5 shows the detections (TS > 9) and 95% CL upper limits that result from this analysis. Statistically significant solar

emission up to ∼1 GeV is apparent for the March 7 flare. Also shown in Figure 5 are the best-fitting photon spectral forms for the pion-decay, exponential cutoff, and power-law models. The insets show the likelihood profiles of the pion-decay model as a function of the proton spectral index.

For the March 7 flare, the best-fit index for a power-law photon model is $\Gamma \sim 2.56 \pm 0.06$, but this clearly does not provide a good fit to the data. Including the exponential cutoff makes a statistically significant improvement, with a $\Delta TS = 96$. In this case, the power-law component has an index of $\Gamma \sim 1.5 \pm 0.3$ and $E_{co} \sim 130 \pm 20$ MeV. It is apparent from Figure 5 that the exponential cutoff model with these parameters is similar in shape to the pion-decay model. The best fit for the March 7 flare is obtained with the pion-decay model with proton index $s \sim 4.5 \pm 0.2$. Integrating the best-fitting photon spectrum from 100 MeV to 10 GeV, the flare-averaged γ-ray flux is $F(100\ \mathrm{MeV}–10\ \mathrm{GeV}) \sim (2.1 \pm 0.1) \times 10^{-5}$ photons cm^{-2} s^{-1}, which corresponds to an energy flux of $(7.2 \pm 0.4) \times 10^{-9}$ erg cm^{-2} s^{-1}. For the duration of the γ-ray emission, about 13.3 hr, the total emitted energy >100 MeV is $\mathcal{E}_\gamma \sim (9.7 \pm 0.5) \times 10^{23}$ erg.

For the June 7 flare, the best-fit photon index for the power-law model is $\Gamma \sim 2.45 \pm 0.09$, but the exponential cutoff model is preferred (with a $\Delta TS = 44$). In this case, $E_{co} \sim 210 \pm 40$ MeV. For the pion-decay model, the best-fit proton index is $s \sim 4.3 \pm 0.3$, similar to the March 7 flare within uncertainties. Using this model, the average 100 MeV to 10 GeV flux is $(3.1 \pm 0.2) \times 10^{-5}$ photons cm^{-2} s^{-1}, corresponding to an energy flux of $(10 \pm 1) \times 10^{-9}$ erg cm^{-2} s^{-1}. The total emitted energy >100 MeV over the 36 minutes of detection of the flare was $\mathcal{E}_\gamma \sim (6.0 \pm 0.6) \times 10^{22}$ erg.

The March 7 event was sufficiently strong that we could study spectral evolution. We carried out the spectral analysis method for each of the five time intervals in Table 2. For no time interval other than the last one, where the emission is weak, was the simple power-law model an adequate fit to the data. The first four time intervals are well described by the pion-decay model and show a significant, monotonic softening in time of the proton spectrum responsible for the γ-ray emission. The best-fit proton spectral indices and the corresponding integrated 100 MeV to 10 GeV fluxes are given in Table 2.

3.4. Multi-wavelength and Proton Data

Both flares were observed with instruments in X-rays, extreme-ultraviolet (EUV), and radio, as well as by charged-particle detectors. They were both modest *GOES* M-class flares with no *RHESSI* HXR signal above 300 keV,[67] and both were associated with SEEs. The light curves of the *GOES* 0.1–0.8 nm band, the *RHESSI* 25–50 keV channel, and *GOES* proton data are plotted below the *Fermi* LAT light curves in Figures 1 and 2. For the March 7 event, we note additional peaks in the *GOES* X-ray light curves that correspond to flares from ARs other than that producing the M3.7 flare: AR 11166, 11165, 11171. For the M3.7 flare starting at 19:43 UT on March 7, the impulsive phase lasted about 15 minutes, and the HXR and soft X-ray emissions have light curves and intensities typical of many flares. The bremsstrahlung HXR emission indicates acceleration of electrons at least to 1 MeV. The total energy in 20–300 keV HXRs integrated over the impulsive phase is $\mathcal{E}_{HXR} \sim 1.7 \times 10^{25}$ erg, ∼20 times larger than the energy $\mathcal{E}_\gamma(E > 100\ \mathrm{MeV})$ integrated over the 13.3 hr of γ-ray emission (from Section 3.3).[68] *RHESSI* imaging of the March 7 flare shows an unusually long ($\sim 10^{10}$ cm) soft X-ray loop with strong emission from two footpoints and weak emission >20 keV from the top of the loop. For the June 7 flare, the HXR flux >20 keV (calculated from *RHESSI* data) is $\mathcal{E}_{HXR} \sim 9.8 \times 10^{24}$ erg, more than a factor of 100 larger than the energy released at high energy.

SDO/AIA movies at EUV wavelengths show considerable activity and multiple episodes of loop brightening during this flare. SEP proton flux time profiles observed with *GOES* above 30, 50, and 100 MeV are plotted in Figures 1 and 2. There is a significant proton flux above 50 MeV starting about 90 minutes after the March 7 flare, but no significant flux above 100 MeV is apparent. *GOES* proton fluxes for the June 7 flare increased more promptly, were somewhat higher, and extended beyond 100 MeV. Both flares were associated with fast CMEs.[69] For the March 7 flare, the estimated plane-of-sky velocity of the CME is ∼2000 km s^{-1}, and the CME was preceded by an evident shock structure,[70] while for the June 7 flare, the CME velocity was measured to be ∼1000 km s^{-1}.

4. DISCUSSION

During its first 4 yr, the *Fermi* LAT has detected γ-rays above 100 MeV from 18 solar flares, half of which are M-class (see Table 1). This suggests that acceleration of electrons and/or protons up to several GeV energies may be a more common occurrence, in even modest flares, than previously thought from the EGRET observations of three bright X-class flares in 1991 June. The highest energy γ-ray recorded from the 2011 March 7 flare has an energy of ∼1 GeV. If this is due to pion decay, it requires protons of energies ∼5 GeV since the mean energy of γ-rays from π^0 decay is typically ∼1/5 of the proton energy (in the relativistic limit) (Gaisser 1991). If the γ-ray emission is due to electron bremsstrahlung, the electron spectrum must extend beyond 1 GeV, with the exact value depending on the electron spectral index.

Thus, continuous monitoring of the Sun with the LAT, in combination with broadband ground-based and space-based observations across the electromagnetic and charged-particle spectrum, can shed new light on the particle acceleration mechanisms in solar flares and perhaps elsewhere.

In this paper, we have described the detailed analysis of the first two long-duration solar flares observed with *Fermi* LAT: those of 2011 March 7 and June 7. With 13.3 hr of γ-ray emission, the March 7 flare is longer than any of the flares observed with EGRET. Unlike those earlier long-duration γ-ray flares associated only with *GOES* X-class flares (Ryan 2000), these two flares were associated with more modest M-class flares. The strong detection of γ-rays >100 MeV composing only a small fraction of the total energy observed in the HXR band demonstrates that the sensitivity of the LAT is providing access to a new range of solar flare phenomena. Our detailed data analysis of these two flares indicates the following.

1. The >100 MeV γ-rays clearly originate from the Sun and appear to be centered with good confidence at the AR responsible for the other flare activity (seen by *RHESSI* and *SDO*). The angular resolution of the LAT does not allow us

[67] http://sprg.ssl.berkeley.edu/~tohban/browser/?show=qlp

[68] This and other results based on *RHESSI* and *SDO* data are from Q. Chen et al. 2013, private communication.

[69] http://cdaw.gsfc.nasa.gov/CME_list/

[70] http://www.spaceweather.com/archive.php?view=1&day=08&month=03&year=2011

to resolve spatially the details of the emission, leaving open the question of the size and geometry of the source region.

2. Although the Sun was not in the *Fermi* LAT FOV during the impulsive phases of these flares, simple extrapolation of the observed light curve of the March 7 flare back to the impulsive phase suggests that significant γ-ray emission may have been present then. The comparison between the number of detections of impulsive phases ("Type I" in Table 1) and the number of flares with no impulsive phase detected ("Type D") also suggests that this may indeed be the case.
3. The shock front of a CME is known to accelerate SEPs, sometimes to energies >300 MeV required for γ-ray production (Reames 2013), but its contribution to the acceleration of the particles that produce γ-rays remains unclear. It is believed that there exists a "reservoir" of accelerated particles downstream of the shock behind the CME (Reames 2012, 2013; Zank et al. 2000, 2007), which could produce γ-rays. However, γ-ray production cannot take place at the reservoir because of prevailing low densities ($\ll 10^{10}$ cm^{-3}). The accelerated protons and electrons must be transported to higher densities below the corona for efficient production of radiation (see below), presumably following some field lines that connect the downstream region to the Sun while the shock front progresses deep into interplanetary space. Whether this is possible is not known, and it is a challenging problem, especially for the 2011 March 7 flare, where, after the 13.3 hr duration of the γ-ray emission, the CME shock front would have traveled more than halfway to the Earth. Thus, acceleration in the corona may be a more attractive explanation, especially considering the relatively large flaring loop seen by *RHESSI* and the extended and complex activity seen by *SDO*. In this case stochastic acceleration by turbulence may be the dominant mechanism (Petrosian & Liu 2004). The *Fermi* LAT observations, when combined with SEP data, provide a unique opportunity to distinguish between these two competing scenarios.
4. It is common to describe long-duration events in the framework of the so-called trap-precipitation model as was done in the analysis of the X12.0 1991 June 11 flare, the longest solar flare observed by EGRET (Kanbach et al. 1993). If the trapping is due to magnetic field convergence, Coulomb collisions cannot be the agent responsible for scattering of the particles into the loss cone and their precipitation, because for >100 MeV electrons and essentially all non-thermal protons, the Coulomb pitch-angle scattering time is much shorter than the Coulomb energy loss time. Scattering by turbulence is another possibility, but as shown in Table 2 for the pion-decay model and the electron bremsstrahlung model, we observe a gradual softening of the proton spectrum during the 2011 March 7 flare. This would require a scattering time that decreases with energy (high-energy particles escape and radiate first), which is not expected in scattering by turbulence, unless the turbulence spectrum is much steeper than Kolmogorov (see Pryadko & Petrosian 1997). Thus, trapping is an unlikely scenario.
5. The spectral analysis shows that the γ-ray spectra cannot be well fit by a simple power law, while including an exponential cutoff provides an acceptable fit. Thus, if electron bremsstrahlung is responsible for the observed γ-rays, this requires a similar spectrum for the electron population. A model based on decay of pions produced by interactions of accelerated protons (and α particles) having a power-law spectrum with background particles provides an equally acceptable fit. We cannot distinguish spectroscopically between electron bremsstrahlung and the pion-decay models. However, for emission mechanisms in the corona-chromosphere, electron bremsstrahlung seems unlikely. For typical flare densities and magnetic fields, most (>90%) of the >100 MeV electron energy would appear as submillimeter and far-infrared emission via the synchrotron process and ~50 keV HXRs via inverse-Compton scattering of solar optical photons. This fraction would be even higher at the lower densities expected for the large loop seen by *RHESSI*. In addition, acceleration of electrons to the GeV range would require acceleration timescales shorter than a few seconds to overcome the rapid synchrotron loss rate. On the other hand, if >100 MeV electrons are not trapped above the transition region and penetrate deep into the solar atmosphere, they will lose energy primarily via bremsstrahlung. Whether the bremsstrahlung origin of the γ-rays can be definitely ruled out by existing observations requires a more detailed analysis beyond the scope of this paper. The pion decay scenario seems more plausible and requires only a moderate energy input. As mentioned above, the total energy in long-duration γ-rays above 100 MeV is several hundred times less than that of the HXRs observed with *RHESSI* during the short impulsive phase. A detailed analysis of efficiency of pion-decay γ-ray production is beyond the scope of this paper.

In summary, the *Fermi* LAT observations of the locations, spectra, and evolution of solar flares in the >100 MeV energy range have raised interesting issues regarding acceleration, transport, and radiation of particles in solar flares. The *Fermi* LAT Collaboration will continue to monitor the Sun through the peak of Solar Cycle 24.

The *Fermi* LAT Collaboration acknowledges generous ongoing support from a number of agencies and institutes that have supported both the development and the operation of the LAT, as well as scientific data analysis. These include the National Aeronautics and Space Administration and the Department of Energy in the United States; the Commissariat à l'Energie Atomique and the Centre National de la Recherche Scientifique/Institut National de Physique Nucléaire et de Physique des Particules in France; the Agenzia Spaziale Italiana and the Istituto Nazionale di Fisica Nucleare in Italy; the Ministry of Education, Culture, Sports, Science and Technology (MEXT), High Energy Accelerator Research Organization (KEK), and Japan Aerospace Exploration Agency (JAXA) in Japan; and the K. A. Wallenberg Foundation, the Swedish Research Council, and the Swedish National Space Board in Sweden.

Additional support for science analysis during the operations phase is gratefully acknowledged from the Istituto Nazionale di Astrofisica in Italy and the Centre National d'Études Spatiales in France.

We also acknowledge G. Share for his continuous support and important contribution to the *Fermi* LAT Collaboration.

REFERENCES

Abdo, A. A., Ackermann, M., Ajello, M., et al. 2011, ApJ, 734, 116
Ackermann, M., Ajello, M., Albert, A., et al. 2012a, ApJS, 203, 4
Ackermann, M., Ajello, M., Allafort, A., et al. 2012b, ApJ, 745, 144
Allafort, A., Tanaka, Y. T., Omodei, N., & Giglietto, N. 2011, ATel, 3214, 1
Atwood, W. B., Abdo, A. A., Ackermann, M., et al. 2009, ApJ, 697, 1071

Brueckner, G. E., Howard, R. A., Koomen, M. J., et al. 1995, SoPh, 162, 357
Esposito, J. A., Bertsch, D. L., Chen, A. W., et al. 1999, ApJS, 123, 203
Fermi-LAT Collaboration 2013, arXiv:1304.5559
Gaisser, T. K. 1991, Cosmic Rays and Particle Physics (Cambridge: Cambridge Univ. Press)
Gehrels, N. 1986, ApJ, 303, 336
Kanbach, G., Bertsch, D. L., Fichtel, C. E., et al. 1988, SSRv, 49, 69
Kanbach, G., Bertsch, D. L., Fichtel, C. E., et al. 1993, A&AS, 97, 349
Kerr, M. 2011, arXiv:1101.6072
Lande, J., Ackermann, M., Allafort, A., et al. 2012, ApJ, 756, 5
Lin, R. P., Dennis, B. R., Hurford, G. J., et al. 2002, SoPh, 210, 3
Mattox, J. R., Bertsch, D. L., Chiang, J., et al. 1996, ApJ, 461, 396
Meegan, C., Lichti, G., Bhat, P. N., et al. 2009, ApJ, 702, 791
Murphy, R. J., Dermer, C. D., & Ramaty, R. 1987, ApJS, 63, 721
Nolan, P. L., Abdo, A. A., Ackermann, M., et al. 2012, ApJS, 199, 31
Pelassa, V., Preece, R., Piron, F., et al. 2010, arXiv:1002.2617
Petrosian, V., & Liu, S. 2004, ApJ, 610, 550
Pryadko, J. M., & Petrosian, V. 1997, ApJ, 482, 774
Ramaty, R., & Mandzhavidze, N. 1994, in AIP Conf. Proc. 294, High-Energy Solar Phenomena—A New Era of Spacecraft Measurements, ed. J. Ryan & W. T. Vestrand (Melville, NY: AIP), 26
Rank, G., Ryan, J., Debrunner, H., McConnell, M., & Schönfelder, V. 2001, A&A, 378, 1046
Reames, D. V. 2012, ApJ, 757, 93
Reames, D. V. 2013, SSRv, 175, 53
Ryan, J. M. 2000, SSRv, 93, 581
Tanaka, Y. T., Omodei, N., Takahashi, H., Grove, E., & Ciprini, S. 2011, ATel, 3417, 1
Trottet, G., Vilmer, N., Barat, C., et al. 1998, A&A, 334, 1099
Zank, G. P., Li, G., & Verkhoglyadova, O. 2007, SSRv, 130, 255
Zank, G. P., Rice, W. K. M., & Wu, C. C. 2000, JGR, 105, 25079